

STRUCTURAL AND OPTICAL PROPERTIES OF Cr-SUBSTITUTED Mg-FERRITE SYNTHESIS BY CO-PRECIPIATION METHOD

S. IMRAN^a, N. AMIN^b, M. I. ARSHAD^b, M.U. ISLAM^c, H. ANWAR^d,
A. AZAM^d, M. AHMAD^e, M. FAKHAR- E-ALAM^b, G. MURTAZA^c,
G. MUSTAFA^{c*}

^aDepartment of Physics, Allama Iqbal Open University Islamabad, Pakistan

^bDepartment of Physics, G.C University Faisalabad, 38000, Pakistan

^cDepartment of Physics, BahauddinZakariya University Multan 60800, Pakistan

^dDepartment of Physics, University of Agriculture Faisalabad, Pakistan

^eDepartment of Physics, COMSATS Institute of Information Technology, Lahore-54000, Pakistan

A series of Cr substituted Mg-ferrites were synthesized by coprecipitation technique annealed at 900 °C for 6h. XRD analysis technique was used to confirm the formation of synthesized ferrites structure and the particle size estimated by Scherrer formula was found to be lying in the range 42.4 to 84.8 nm. All the prepared samples exhibited inverse cubic spinel structure and lattice parameter found in the range (8.3814-8.3756 Å). The morphology and the formation of nanoparticles were observed by scanning electron microscopy (SEM). For the elemental analysis, the energy dispersive X-ray (EDX) confirmed the existence of Mg, Cr, Fe and O orbital state. Moreover, the representative sample UV/Vis spectra of the Cr-substituted Mg-ferrites revealed that the absorbance shifted from 373 to 386 nm for reference samples at x=0.2 and x =0.5 and the wavelength lies most prominently in UV region wavelength 200-380 nm approximately. The electrical measurements were done by two probe method. It was observed that at room temperature the DC resistivity decreased with the increase in chromium content while synthesized material have semiconductor behavior with the rise of temperature.

(Received August 16, 2016; Accepted November 5, 2016)

Keywords: Spinel ferrites; co-precipitation; X-ray diffraction; DC conductivity

1. Introduction

Ferrites have an important group of magnetic materials with a wide range of applications due to their small dielectric loss and magnetic properties. These spinel ferrites of chemical formula MFe_2O_4 play a significant part in microwave control components such as isolators, phase shifters and circulators. For the high frequency applications ferrites like Mg-Cr were considered as the most versatile due to their low eddy currents and high resistivity. Optical properties and Microstructure of Mg-Cr ferrites are very sensitivity to chemical compositions, cation distribution, sintering temperature and time, additive amount of the cations and methods of preparation. The soft-magnetic behavior in ferrites is due to the exchange interaction between the cations on the poly-hedral sites [1-2]. The cubic spinel-structured ferrite represents a well-known and significant class of iron oxide materials [3]. It is concluded in the studies literature survey that the high resistivity makes these spinel ferrites suitable for high-frequency applications where eddy current losses are required to be low, resistivity usually increases with the decreasing grain size, [4]. Moreover, Mg ferrites may be used in conjunction with other divalent ions and trivalent ions (Al and Cr) in high frequency applications for resistivity reasons [4-5]. The synthesized sample have cubic crystalline structure, space group $O7h$ ($Fd3m$) and eight formula units cell. A unit cell contains 8 tetra-hedrons and 16 octa-hedrons. The Mg^{2+} ions are situated on center of the tetra-

* Corresponding authors: ghulammustafabzu@gmail.com

hedron and coordinated by O^{2-} ions with full Td (A site) symmetry while Cr^{3+} ions are located at the centre of the octa-hedrons coordinated by O^{2-} ions with T3d (B site) symmetry. The doped metal ions can substitute either A or B sites or both depending upon its site type and valency. Most of the major magnetic properties of Mg-ferrite strongly depend on the shape doping and size [6]. $MgFe_2O_4$ is an n-type soft magnetic semi conducting material, which deals number of applications in heterogeneous catalysis, sensors, micro-wave devices, adsorption and magnetic technologies its efficiency increases when it doped with Cr or other metals [7]. Structural studies of magnesium-doped ferrites have also been carried out by Widatallah et al [C]. Other researchers have also investigated the effect of Cr in different ferrites system [8-12]. A number of investigations have been reported earlier which describe the influence of divalent ions [8] and trivalent ions (Al, Cr) [9] substitutions in Mg-ferrites on its various properties. Different methods have been adopted to synthesize spinel ferrites including co-precipitation, sol-gel, hydrothermal, micro-emulsion and solid state reaction [13-14]. However, in the process of sample preparation structure can be controlled by cooling and annealing rates. Among the several methods, co-precipitation is one of the best and attractive methods due to its simple experimental arrangement and high yield of ultrafine particles at low sintering temperature [4, 15]. By the addition of a minor amount of impurity leads to effective change in the magnetic and electrical properties of a material. In these ferrites, addition of metal cations of different valence states leads to various tetra-hedral (A) and octa-hedral (B) sites distributions [15-16]. The modification in cation distribution also affects the physical properties of spinel ferrites. Especially, the substitution of transition metal ions and rare-earth ions influences the electrical as well as magnetic properties of $MgFe_2O_4$ [7-9, 17]. In this communication we have reported the effect of Cr^{+3} substitution on the physical, optical and electrical properties of mixed Mg-Cr-ferrites.

2. Materials and Methods

2.1. Samples synthesis, preparation and equipments

The chemical reagents including $Mg(NO_3)_2 \cdot 6H_2O$, $Cr(NO_3)_3 \cdot 9H_2O$, $Fe(NO_3)_3 \cdot 9H_2O$ (Aldrich, 99%), and ethanol were used to prepare the samples with formula $MgCr_xFe_{2-x}O_4$ (where $0 < x < 0.10$) with interval 0.02 by co-precipitation method. The procedure of the synthesis is described in previous research work [18-19]. The X-ray diffraction (XRD) patterns were obtained at room temperature by (Xpert Pro PANalytical diffractometer). In addition morphology of the samples was studied by scanning electron microscope (SEM) model (JSM-6490 JEOL). The elemental analysis of the representative sample was carried out by energy dispersive peak using energy dispersive X-ray spectroscopy EDXS, Model (JFC-1500 JEOL). UV-Vis absorption spectra were obtained using a UV-Vis-NIR spectrophotometer (PerkinElmer Lambda 9) at room temperature. Moreover, dc electrical resistivity measured by a two-point probe method with a Keithley electrometer model 2400 which was connected in a series with sample holder at 280 K to 400 K.

3. Results and Discussions

3.1. Crystal Structure Analysis

Fig.2 shows the X-ray diffraction patterns of $MgCr_xFe_{2-x}O_4$ (where $0 < x < 0.10$) ferrite system synthesized through co-precipitation technique for the thermal treatment of 900 °C for 6 h. From the patterns no other phase has been detected and for all the samples the diffraction lines are found to be sharp which are consistent with face-centered cubic spinel structure. Moreover, diffraction peaks corresponding to the planes (220), (311), (222), (400), (422), (511/333), (440) confirm the synthesis of spinel ferrite structure. The Jade 5 software was used to index all the peaks. The lattice parameters 'a' was calculated using the relation [20].

$$a = \frac{\lambda}{2\sin\theta} \sqrt{(h^2 + k^2 + l^2)} \quad (1)$$

The values of lattice parameters have been calculated by using the d-spacing values and the respective Miller indices (hkl) from the formula as given in Eq.1. The results show that, lattice parameters are decreased with the increase of Cr^{3+} contents which can be explained on the bases of difference in ionic radii of Fe^{3+} and Cr^{3+} . The smaller ionic radius Cr^{3+} (0.63 Å) exchanges the larger crystal radius Fe^{3+} (0.64 Å), likewise the lattice parameters decreases due to shrinkage of unit cell dimensions, which causes dilation of the host spinel lattice constant $a = 8.354 \text{ \AA}$ as compared to pure sample. Furthermore, it is observed that for $x = 0.04$ ($a = 8.3826 \text{ \AA}$) and $x = 0.06$ ($a = 8.3775 \text{ \AA}$) which decreases the lattice constant. The site preference of Cr^{3+} ions leads mainly to (B) site therefore, chromium is a normal spinel with chromium ions always in octahedral (B) site. The change in 'a' specifies the structural changes from inverse to certain degree of normal. The unit cell volume determined in cubic spinel ferrites under these condition $a = b = c$ while $\alpha = \beta = \gamma = 90^\circ$.

$$V_{\text{cell}} = a^3 \quad (2)$$

The observed unit cell volume of the spinel cubic ferrites have similar trend as per lattice parameters as listed in the Table1. Fig. 2 (a) shows the variation of unit cell volume and lattice parameters as a function of Cr ion content.

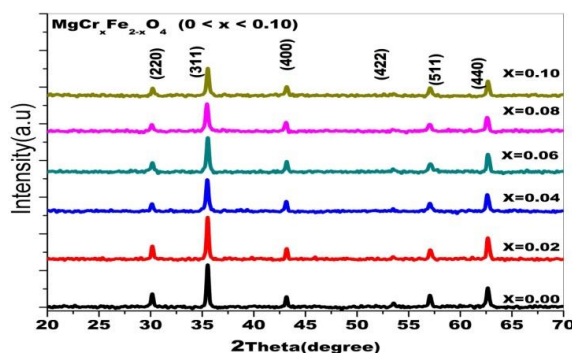


Fig. 3.1 XRD patterns of Cr-substituted Mg-ferrites ($0 < x < 0.10$)

Table 1. Lattice constant, volume of the unit cell, crystallite size (nm), X-ray density (D_x) of Cr substituted Mg-ferrites annealed at temperature 900°C for 6 h

Composition	Lattice constant a (Å)	Volume of the unit cell (\AA^3)	Crystallite size $\langle D \rangle$ (nm)	X-ray density D_x (g/cm^3)
MgFe_2O_4	8.3814	588.775	70.6	4.51
$\text{MgCr}_{0.02}\text{Fe}_{1.98}\text{O}_4$	8.3934	591.308	42.4	4.49
$\text{MgCr}_{0.04}\text{Fe}_{1.96}\text{O}_4$	8.3826	589.028	51.4	4.51
$\text{MgCr}_{0.06}\text{Fe}_{1.94}\text{O}_4$	8.3775	587.954	70.6	4.52
$\text{MgCr}_{0.08}\text{Fe}_{1.92}\text{O}_4$	8.3761	587.659	72.2	4.52
$\text{MgCr}_{0.10}\text{Fe}_{1.90}\text{O}_4$	8.3756	587.554	84.8	4.53

The X-ray density D_x was calculated from the given Eq.4 where, V is primitive unit cell volume, Z denotes 8 molecules per unit cell of the spinel structure, M is the molecular weight of the sample and N_A is the Avogadro's number ($6.02 \times 10^{23} \text{ g/mol}$).

$$\rho_x = \frac{Z M}{N_A V} \quad (3)$$

Table 1 revealed that the X-ray density variation as a function of Cr content can be attributed to the radii of the constituent ions and the atomic weight. The values of X-ray density

were found in range of 4.49-4.53 g/cm³ which may be due to inhibition of grain growth by the substitution of Cr³⁺ into the spinel lattice. The analysis of the crystallite size (D) nm of the synthesis spinel ferrites samples which have single phase determined by using the Scherer's formula (Eq.4), where k is the coefficient of shape have value between 0.9 to 1.0, λ is the X-ray wavelength, B is the full width at half maximum of each Phase and θ_B is the Bragg's diffraction angle [21].

$$D = \frac{k \lambda}{B_{(hkl)} \cos \theta_B} \quad (4)$$

From the XRD data, the crystallite size is calculated by Eq.4 and found as 70.6 nm for pure sample ($x=0.00$) while the sample $x=0.2$ to $x=0.10$ with the increasing Cr content, the average crystallite size observed in the ranges are 42.4-84.8 nm (Table 1) due to the grain boundary mobility. It has been reported that the crystallite size ≤ 50 nm is required to obtain the suitable signal to noise ratio in the high density recording media [22-23]. In the current work the crystallite size is 42.4 nm ($x=0.02$) so this sample can be used for in high density recording media applications in attaining suitable signal to noise ratio.

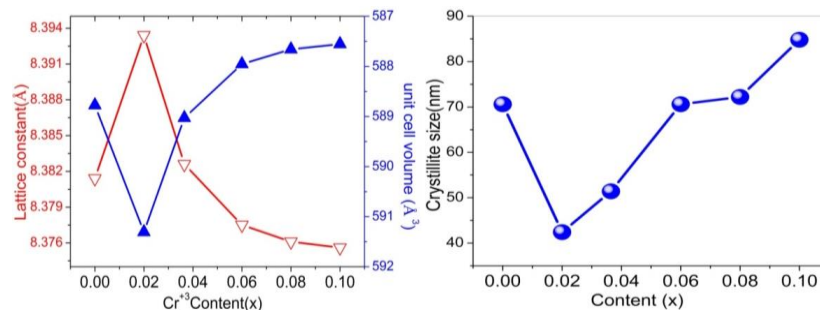


Fig. 3.2. (a) Relation of content ($0 < x < 0.10$) with lattice constant and unit cell volume (b) Relation of Cr content vs. crystallite size (nm).

3.2 Morphology and Elemental analysis:

Fig.3.3 shows the SEM micrographs of representative samples $x=0.02$, $x=0.04$. The micrographs of the sample $x=0.04$ exhibit the homogeneous grain size distribution and seems to be spherical shapes. The agglomerates are observed in the investigated ferrite samples, the presence of these agglomerates may be found due to sintering process as an outcome of chemical reaction. Relatively weak Vander Waals bonds or magnetic forces even might be responsible to hold these agglomerates together [24].

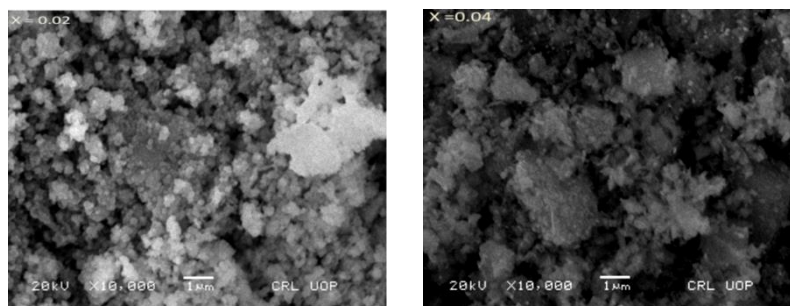


Fig. 3.3 SEM Micrographs for Cr-substituted Mg-ferrites at $x=0.02$ and 0.04

Fig.4. shows the energy dispersive spectrum of pure and Cr substituted MgFe₂O₄ for different concentrations. The observed atomic and weight percentages of Mg, Fe, O and Cr

elements in the prepared nanoparticle samples are shown in the inset tables of Fig. 3.4 from EDX analysis, it was confirmed that no impurity is present in the prepared samples.

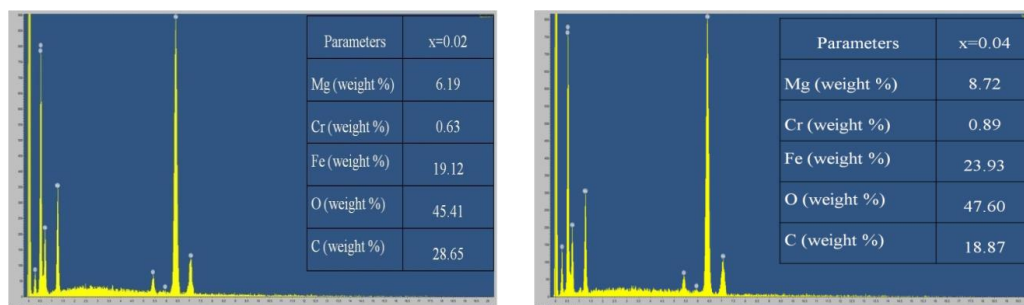


Fig. 3.4 EDX Spectrum of the Cr-substituted Mg-ferrites at $x = 0.02$ and $x = 0.04$

3.3 Optical Properties:

Figure 3.5a illustrates the UV/Vis spectra of the Cr-substituted Mg-ferrites, the absorbance decreases as the doping of Cr^{+3} is increased and the wavelength lies most prominently in UV region wavelength 200-380 nm approximately an intense peak at 470.6 nm points toward the excitation of π electrons in the spinel cubic structure. Another absorption edge appears at 1076 nm representing the presence of oxygen-containing groups linked with a cubic structure. An additional peak was noted at 1076 nm and it could be due to the presence of ZnO , Cr_2O_3 and Fe_3O_4 oxides. Moreover, in the spectrum, due to the reduction of Cr-substituted Mg-ferrites absorption peak at 230 nm was red shifted to 268 nm.

3.3.1 Band gap

The optical band gap and the absorption coefficient (α) of the synthesized ferrites is calculated by Eq. (5) [25].

$$\alpha hv = A(hv - E_g)^n \quad (5)$$

where ' α ' is the linear absorption coefficient of the material, hv is the photon energy 'A' is a constant of proportionality, E_{gap} is the optical band gap energy and 'n' is a constant related with different kinds of electronic transitions ($n = 1/2$ and 2 for a direct and indirect allowed respectively).

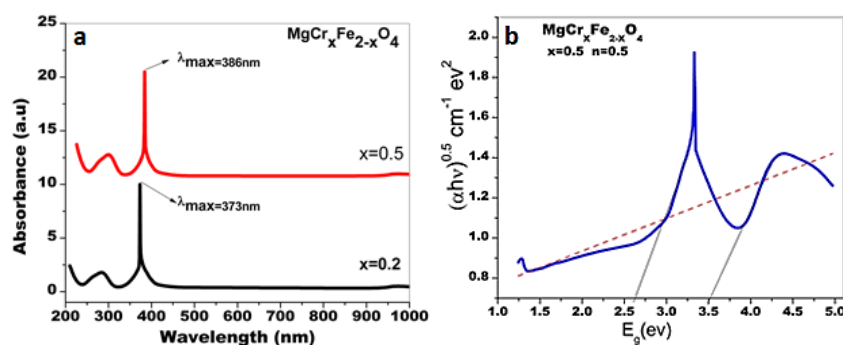


Fig. 3.5 (a) Absorbance spectra of Cr-substituted Mg-ferrites at $x=0.2$ and $x=0.5$. (b) The optical band gap and the absorption coefficient of the synthesized ferrites

The value of E_g of the prepared sample for $x = 0.08$ is calculated by plotting Tauc's graphs between $(\alpha hv)^2$ versus (hv) photon energy as shown in Fig.3.5b The intercept of the graph linear

region on energy axis at $(\alpha h\nu)^2$ equal to zero gives the band gap energy. The observed band gap energy values are found to be (2.5eV and 3.5eV) in the product material; such kinds of behavior may be due to lattice defects, the grain boundary diffusion produced the displacement of atoms and line defects. Moreover, it is observed that the energy band gap increases whenever the particle size decreases.

3.4 Current-voltage measurements

For Cr substituted Mg-ferrites the current voltage (I-V) measurements were carried out using Keithley electrometer model 2400. In the I-V curves for all samples are given in Fig. 3.6 (a & b) which recorded at 5V and 15V from these curves the DC resistivity of each sample is calculated from the following relation [26].

$$\rho = \frac{RA}{d} \quad (6)$$

Where (d) is the thickness of pellet while (A) is the area of electrode in contact with the sample. The electrical resistivity depends on the crystal structure and composition of the material [27].

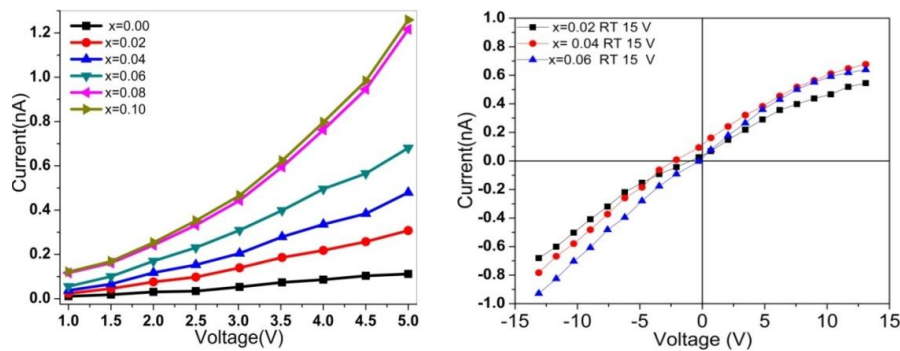


Fig 3.6 (a) Variation of voltage and current for Cr substituted Mg-ferrite (15V),
(b) Variation of voltage and current for different concentration of Cr substituted Mg-ferrite

The Fig.3.7 shows that the values fluctuate by increase in the concentration of Cr in synthesized material. The compositional dependence of dc electrical resistivity of the investigated samples which is raise (decrease in conductivity) all samples show a linear trend with the increase in Cr-contents due to which the iron ions become deficient at (B) site. Such behavior of dc electrical resistivity for samples of the ferrite has also been reported at room temperature [28].

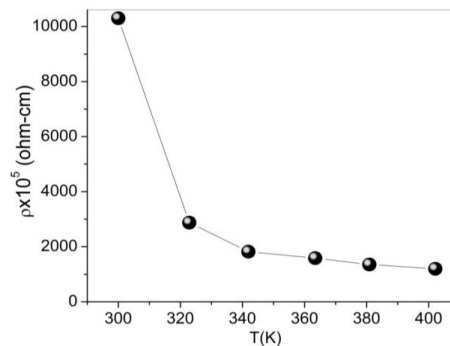


Fig. 3.7 Variation of dc resistivity of Cr substituted Mg-ferrite with temperature.

The reason, of the increasing attitude in DC electrical resistivity with the increase of Cr-concentration is due to the decrease of number of $\text{Fe}^{+3}/\text{Fe}^{+2}$ ions pairs at octa-hedral (B) sites. Moreover, the number of iron ions at B-sites start to decrease when Cr ions replace the iron ions at

the octa-hedral site, consequently, the number of hopping electrons decrease and increase in the electrical resistivity. Fig.3.7 explains the variation of dc resistivity with temperature range between 300K and 400K. Here resistivity plotted versus temperature (K) revealed that the resistivity of the synthesized sample decreases with increasing temperature, a behavior of a typical semiconductor.

4. Conclusions

In this study, Cr-substituted Mg-ferrite of ($x=0.0$ and $x = 0.1$) have been prepared successfully by using Co-precipitation technique. The structure of the samples was confirmed by XRD and SEM. Crystallite size of the product was found in the range 42.4 to 84.8 nm. Scanning electron microscopy showed spherical morphology with soft agglomeration and narrow size distribution of the nanoparticles. As the doping of Cr^{+3} is increased the UV/Vis spectra of the prepared samples reveals that the absorbance decreases. Electrical properties showed that DC resistivity have inverse relation with Cr-concentration and temperature, a behavior of a typical semiconductor.

Acknowledgements

Corresponding author (Ghulam Mustafa) is thankful to Dr Akbar Alifor providing the experimental facilities at COMSATS Institute of Information Technology, Lahore, Pakistan

References

- [1] R. Tadi, K. Yong-II, A.K. Sarella, C.G. Kim, K.S. Ryu, J. Magn. Mater., **322**, 3372 (2010).
- [2] E. MelaGiriyappa, H.S. Jayanna, J. Alloys Compd. **482**, 147 (2009).
- [3] E. Rezlescu, N. Rezlescu, C. Pasnicu, M. L. Craus, D. P. Popa, J. Magn. Mater., **117**, 448(1992).
- [4] Z. Zi, Y. Sun, X. Zhu, Z. Yang, J. Dai, W. Song. J. Magn. Mater., **321**, 1251 (2009).
- [5] K. Maaz, A. Mumtaz, S. Hasanain, A. Ceylan. J. Magn. Mater. **308**, 289 (2007)
- [6] G. Li, L. Wang, W. Li, R. Ding, Y. Xu. Phys. Chem. Chem. Phys. **16**, 12385 (2014).
- [7] S.K. Pradhan, S. Bid, M. Gateshki, V. Petkov. Mater. Chem. Phys., **93**, 224 (2005)
- [8] K. Seshan, A.S. Bommannavar, D.K. Chakrabarty. J. Solid. State. Chem. **47**, 107(1983)
- [9] K.B Modi, N.N Jani, R.G Kulkarni J. Mater. Sci., **31**, 1311 (1996)
- [10] R.A. Brand, H.G. Gibert, J. Hubsch, J.A. Hellen. J. Phys. F: Met. Phys., **15**, 1987 (1985)
- [11] N.N. Jani, B.S. Trivedi, H.H. Joshi, G.K. Bichile, R.G. Kulkarni. Bull. Mater.Sci., **21**, 223 (1998)
- [12] A.D. Balaev, O.A. Bayukov, A.F. Savitskh. Phys. Status Solidi B, **152**, 639 (1989)
- [13] W.A. Bayoumy, M.A. Gabal. 2010. J. ALLOY. COMPD. **506**, 205 (2010).
- [14] Z. Zi, Y. Sun, X. Zhu, Z. Yang, J. Dai, W. Song. J. Magn. Mater. **321**, 1251 (2009)

- [15]S. Singhal, S. Jauhar, J. Singh, K. Chandra and S. Bansal.J. MOL. STRUCT. **1012**,182 (2012)
- [16]K. Maaz, W. Khalid, A. Mumtaz, S.K. Hasanain, J. Liu, J.L. Duan, Physica E, **41**, 593 (2009)
- [17] A. Rana, O.P. Thakur, V. Kumar, Mater. Lett.**65**, 3191(2011)
- [18]N. Amin, M. Imran Arshad, M. U. Islam, A. Ali, K. Mahmood,G. Murtaza , M. Ahmad, G. Mustafa,Digest Journal of Nanomaterials and Biostructures,**11**(2), 579 (2016)
- [19] G. Mustafa, M.U. Islam, W. Zhang, Y. Jamil, A.W. Anwar, M. Hussain, M. Ahmad, J. Alloys Comp. **618**, 428 (2015).
- [20] H. Mohan, I.A. Shaikh, R.G. Kulkarni, Physica B, **217**, 292 (1996)
- [21]P.S. Aghav, V.N. Dhage, M.L. Mane, D.R. Shengule, R.G. Dorik, K.M. Jadhav, Physica B **406**, 4350 (2011)
- [22]P.P. Hankare, V.T. Vader, N.M. Patil, S.D. Jadhav, U.B. Sankpal, M.R. Kadam, B.K. Chouguleb, N.S. Gajbhiye.,**113**, 233 (2009)
- [23] A.K.M. Zakaria, F. Nesa, M.A. Saeed Khan, S.M. Yunus, N.I. Khan, D.K. Saha, S.G. Eriksson. J. Bangla. Acad. Sci., **39**, 1 (2015)
- [24] D.M. Parikh, Handbook of Pharmaceutical Granulation, (Taylor & Francis Group, LLC Technology, 2005) pp, 1-613
- [25] Yang, S. Y. *et al.* Above-bandgap voltages from ferroelectric photovoltaic devices. Nature Nanotech. **5**, 143 (2010).
- [26] P. Singh, O. Parkash, Devendra Kumar. DC conduction behavior of niobium doped barium stannate, J. Mater. Sci. Mater. Electr, **16**, 145 (2005)
- [27]M. Bhandare, G. Wagh. Int. j. innov. res. sci. eng. technol. (An ISO 3297: 2007 Certified Organization) 5, (2016)
- [28] N. Rezlescu, E. Rezlescu.Solid State Commun.**88**, 139 (1993).